Magnetocaloric Properties of a Charge Ordered $Pr_{0.48}Sr_{0.52}MnO_3$ Perovskite Near First and Second Order Magnetic Transition

Ajay Kumar Saw[1], John Peter J. Nunez[2], Ravi. L. Hadimani[2], and Vijaylakshmi Dayal[1]

[1]Department of Physics, Maharaja Institute of Technology Mysore, (VTU-Belagavi), Mandya 517477, India
[2]Department of Mechanical and Nuclear Engineering, Virginia Commonwealth University, Richmond, VA 23285 USA

Polycrystalline $Pr_{0.48}Sr_{0.52}MnO_3$ forms a tetragonal structure belonging to the I4/mcm space group. X-ray absorption spectroscopy revealed Mn_3d level splitting with a higher density of state in $e_g \downarrow$. The temperature-dependent electrical resistivity plot indicates metal-to-insulator transition (T_{MI}) at 224 K at 0 T. Additionally, at lower temperatures, a distinct thermal hysteresis during heating and cooling cycles between 0 and 2 T fields specifies a first-order (FOPT) magnetic phase transition. The temperature-dependent magnetization plot shows a second-order (SOPT) paramagnetic (PM) to ferromagnetic (FM) transition phase transition at 226 K ($=T_c$) followed by FM to antiferromagnetic (AFM) transition with distinct thermal hysteresis evidence of FOPT at 152.5 K ($=T_N$). The maximum isothermal entropy change (ΔS_M) estimated using Maxwell's model near SOPT is −3.67 J/kg K at 8 T. Moreover, near FOPT the maximum ΔS_M of value +4.29 J/kg K at $H = 4$ T is determined, which thereafter remained constant up to 8 T magnetic field. The ΔS_M value at a lower magnetic field is also computed using the phenomenological model. Landau's theory suitably explains the magnetocaloric (MCE) of $Pr_{0.48}Sr_{0.52}MnO_3$ near SOPT in agreement with the value obtained using Maxwell's relation.

***Index Terms*— XXXXX.** Manganite; Antiferromagnetic; Ferromagnetic; Colossal Magnetoresistance (CMR); Magnetic Entropy Change; X-ray absorption spectra (XAS)

I. Introduction

MANGANITES near half doping are extremely fascinating since competing ferromagnetic metallic (FM-M) and antiferromagnetic (AFM) charge-ordered insulating (COI) phases have an analogous energy scale, implying that both phases potentially coexisted [1]. Furthermore, magnetocaloric (MCE) behavior has been demonstrated in these manganites. Magnetic refrigeration tools, focusing on MCE, is environmentally sustainable and energy efficient than traditional gas compression or expansion refrigeration tools [2], [3], [4]. The MCE, or adiabatic change in temperature (ΔT_{ad}) or isothermal change in magnetic entropy (ΔS_M), is largely been studied in the ferromagnetic (FM) materials at temperatures near second-order (SOPT) paramagnetic (PM) to FM phase transition (SOPT), the AFM materials with first-order (FOPT) FM to AFM-COI phase transition (FOPT) are also investigated for its giant MCE and large ΔS_M values [5], [6], [7], [8], [9], [10], [11], [12]. In this article, we investigated the magneto-transport, magnetic phase transition, and MCE properties of polycrystalline $Pr_{0.48}Sr_{0.52}MnO_3$ synthesized using the solid-state technique.

II. Results and Discussion

A. Structural and Morphological Study

The X-ray diffraction (XRD) plot together with the Rietveld refined pattern of the synthesized samples is shown in Fig. 1.

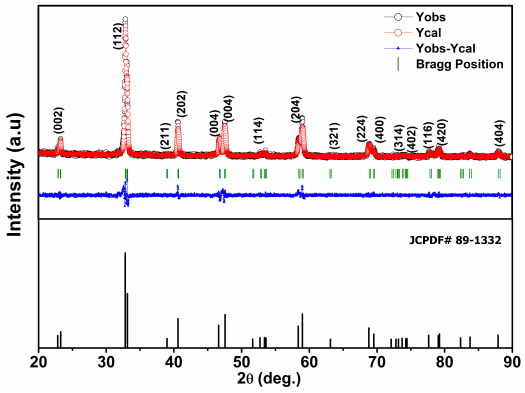

Fig. 1. Experimental XRD pattern along with Rietveld refined pattern.

The pattern suggests the crystallization of the sample in the tetragonal phase (JCPDF# 89–1332) with space group I4/mcm without any secondary phase. The Rietveld refinement was performed using Fullprof software [13]. The lattice parameters acquired using the refinement are, $a = b = 5.407(7)$ (Å), $c = 7.765(2)$ (Å), $V = 227.079(4)$ (Å)^3, Mn-O_1 = 1.941(4) (Å) and Mn_1-O_2-Mn_1 = 126.258 (2)°.

Fig. 2 displays X-ray absorption spectra (XAS) performed at the Mn L edge. The Mn $L_{2,3}$ edge noted in XAS results from the transition of Mn $2p_{1/2}$ and Mn $2p_{3/2}$ states to the vacant Mn_3d state. The protocol described by Subias et al. [14] has been adopted to investigate the accurate charge state of Mn.

According to this protocol, the L_2 peaks of the samples have been aligned with the energy position of MnO_2 and Mn_2O_3 and the later position of the L_3 peak has been investigated. It can be seen that the L_3 peak position lies between the L_3

Manuscript received 27 March 2023; revised 8 May 2023 and 29 May 2023; accepted 5 June 2023. Corresponding author: V. Dayal (e-mail: drvldayal@gmail.com).
Color versions of one or more figures in this article are available at https://doi.org/10.1109/TMAG.2023.3286435.
Digital Object Identifier 10.1109/TMAG.2023.3286435

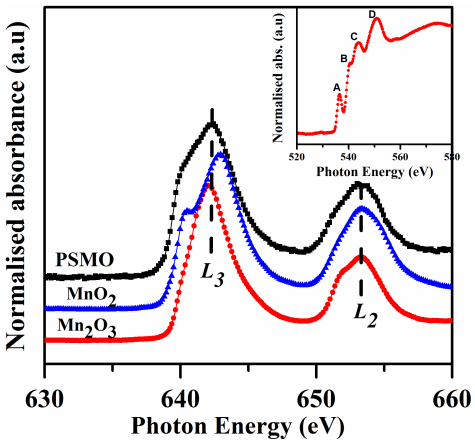

Fig. 2. XAS performed at the MnL edge.

peaks of MnO_2 and Mn_2O_3, suggesting the presence of Mn^{3+} and Mn^{4+} and signifying a mixed valent nature. Additionally, the normalized XAS spectra oxygen $(O)_{1S}$ spectra around the K-edge (in the inset of Fig. 2) show the four distinct bands, where "a" (at 536.52 eV), "c" (at 544.46 eV), and "d" (at 551.25 eV) have been ascribed to the hybridization of O_{2p} with Mn_3d, O_{2p} with Sr_{4d} and O_{2p} with Mn_{4sp}, respectively, whereas "b" (at 540.13 eV), is ascribed to the Mn_3d unoccupied ($e_g \downarrow$) state sensitive to Mn valence, which arises as a result of the splitting of the Mn_3d level. The scanning electron micrograph (SEM) shown in Fig. 3 (left panel) shows densely distributed microns size grains and the energy dispersive X-ray spectrum (EDX) (right panel) suggests the presence of the constituents Pr, Sr, Mn, and O element.

B. Electrical and Magnetotransport Properties

The temperature-dependent resistivity plot as a response to 0 T shown in Fig. 4 shows metal-insulator transition (MI) at $T_{MI} = 224$ K, whereas CO transition at ~150 K.

Additionally, a distinct thermal hysteresis can be seen during heating and cooling cycles between 0 and 2 T field. This hysteresis is a critical feature of a FOPT with the concomitance of AFM and CO phases, designated to the phase transition to the Costate, where ostensibly Mn^{3+} and Mn^{4+} ions display a real space arrangement in the sample [15]. Furthermore, it has been noticed that the applied magnetic field suppressed the resistivity and shifted the T_{MI} at the higher temperature side, indicating that the magnetic field enables the e_g electrons to hop amid the neighboring Mn ions. This hopping strengthens the double exchange (DE) mechanism, which typically favors the FM nature [16]. FOPT is diminished at the higher field (8 T). The temperature-dependent magnetoresistance (MR)%, which is equal to $(\rho H - \rho 0/\rho 0) \times 100$ (as shown in the right scale of Fig. 4) increases by lowering the temperature and applying the magnetic field. MR of ~ 100% has been observed at 5 K and 8 T, which seems to be significant for magnetic device applications. Furthermore, the MR% isotherms, under magnetic fields (0–8 T) are shown in Fig. 5. At 5 and 100 K, the thermal hysteresis in cycles 0–8 T and 8–0 T is seen, which indicates that magnetic fields have caused the CO-I phase to

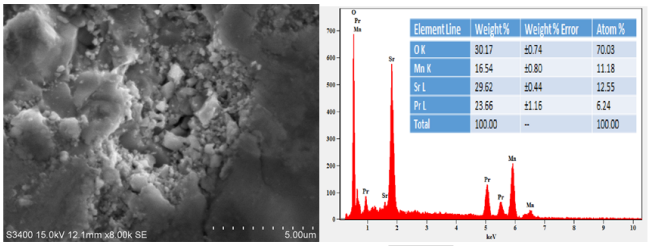

Fig. 3. SEM (left panel) and EDX spectrum (right panel) of the sample.

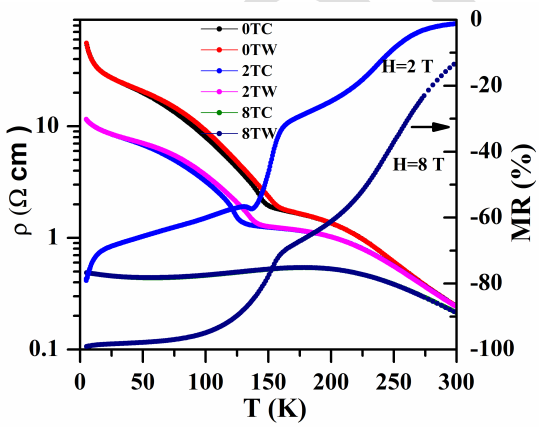

Fig. 4. Resistivity versus temperature plot in left axis and right axis shows MR% versus T.

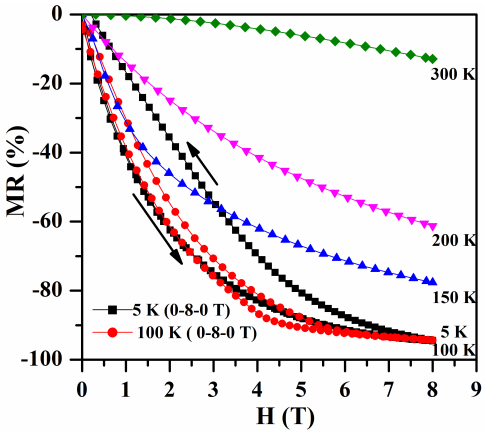

Fig. 5. MR% versus the magnetic field (H) isotherms measured at 5, 100, 150, 200, and 300 K.

destabilize. The dominant low field negative MR along with MR ~ 96% is measured at the temperature at both 5 and 100 K at 8 T. At temperatures well below T_{MI}, it is understood that the FMM phase fraction is significantly greater compared to the COI phase, which results in the low field MR primarily by the grain boundary effect [17], [18].

The adiabatic small polaronic hopping (SPH) model given by (1) is seen to be dominant at a high temperature as shown in Fig. 6 [19], [20], [2]

$$\rho = \rho_0 T_{\exp}\left(\frac{E_a}{K_B T}\right). \quad (1)$$

Here, E_a = activation energy, K_B = Boltzmann's constant, and ρ_0 = residual resistivity coefficient term designated by

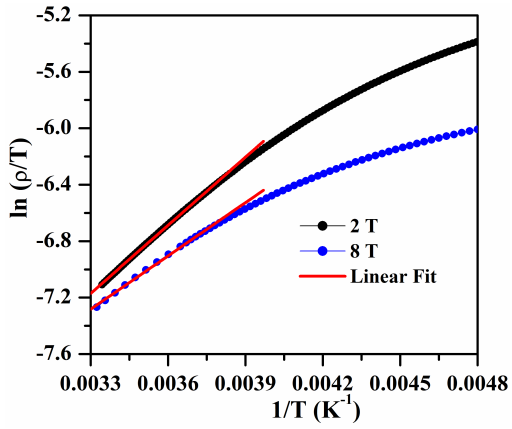

Fig. 6. Plot of $\ln(\rho/T)$ versus 1/T (solid lines indicate linear fits with the SPH model).

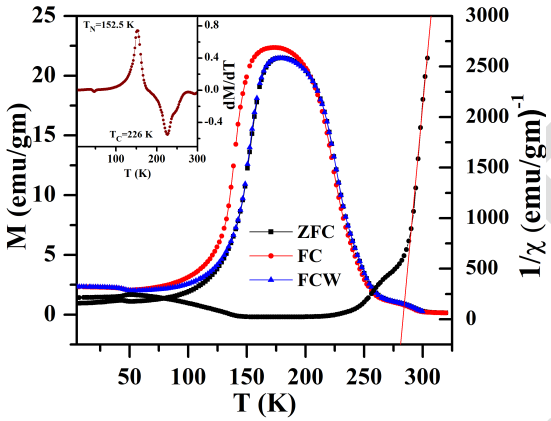

Fig. 7. Temperature dependence of ZFC, FC, and FCW magnetization measured at 500 Oe (Left axis). (Right axis) $1/\chi$ versus T in an applied magnetic field. The inset shows the derivative of magnetization.

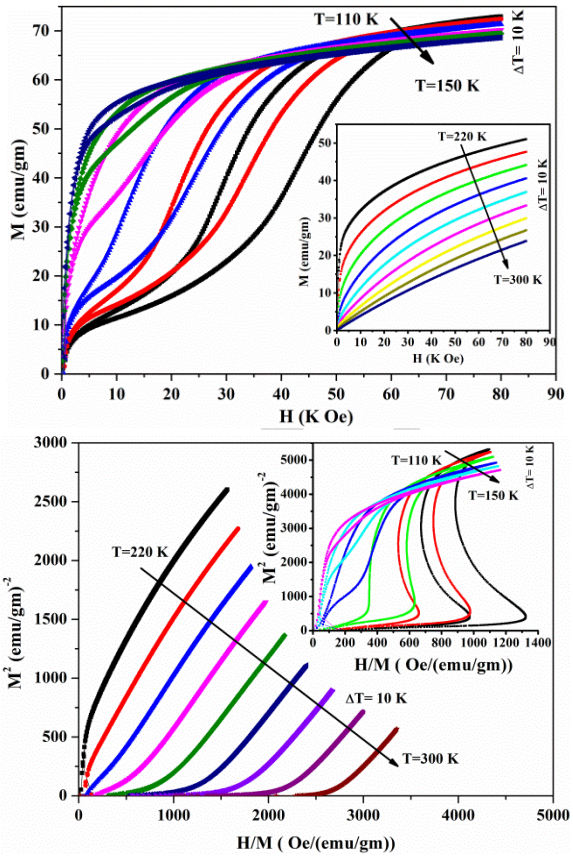

Fig. 8. (Top panel) Magnetic field dependence of magnetization at different temperatures (bottom panel). Arrott's plot at different temperatures.

$\rho_0 = 2K_BT/3ne^2a^2v$, where e = electronic charge, n = density of charge carrier, a = site-to-site hopping distance, and v = longitudinal phonon frequency. The application of the magnetic field decreased the activation energy (E_a) from 138.74 (0 T) to 108.493 meV (8 T).

It is presumed that the application of magnetic decreases E_a value due to a decrease in the distortion of the lattice and the decline in Jahn–Teller electron–phonon coupling, causing the electrons to become delocalized, which is following $\rho(T)$ data, which decreases when the magnetic field is applied.

C. Magnetic and MCE Properties

The zero-field-cooled (ZFC), field-cooled (FC), and FC warming (FCW) magnetization (M) as a response to temperature (T) at 500 Oe magnetic is shown in Fig. 7. The plot shows that the sample undergoes a dual transition; a PM to FM state SOPT at $T_C = 226$ K followed by FM to AFM state (FOPT) at $T_N = 152.5$ K. The Curie–Weiss law fitting to the PM region, the θ_{cw} (=282.6 K) acquired a positive value and corroborates the FM nature of the sample above T_N, however, a slightly higher θ_{cw} value than T_c (226 K) is a signature of a magnetic inhomogeneity in the sample, also higher μ_{eff}^{exp} (3.73 μ_B) than the expected μ_{eff}^{Th} (3.51 μ_B) value confirmed the manifestation of magnetic inhomogeneity just beyond T_c [21], [22].

Furthermore, the magnetic field dependence of magnetization (M versus H isotherms) measured in the temperature range 110–180 K and from 220 to 300 K for a temperature interval of $\Delta T = 10$ K are shown in Fig. 8 (top panel).

It can be noticed that the $M(H)$ data below T_c surges faster at the lower field region and then appears to saturate as the magnetic field is increased. Arrott's plot (M^2 versus H/M) is studied to comprehend magnetic transitions, as shown in Fig. 8 (bottom panel). As per Banerjee [23] criterion, the negative and positive signs of the slope in the Arrotts plot are signatures of the magnetic phase transition resembling FOPT and SOPT, respectively. The magnetic isotherms plot discloses FOPT below 152.5 K and SOPT above 152.5 K in agreement with the temperature-dependent ZFC-FC magnetization measurements.

To further study the MCE behavior, magnetic entropy change (ΔS_M) as a function of temperature and magnetic field has been largely discussed considering various models, such as; phenomenological [24], Maxwell's, and Landau's theory [25]. Using the phenomenological model of the MCE in the magnetic materials at the low field ($H = 0.05$ T), the temperature-dependent magnetization showed ΔS_M to be maximum near $T_N = 152.5$ K, $T_C = 226$ K. Further, in Maxwell's model, based on the thermodynamic theory, the magnetic entropy change (ΔS_M) can be calculated

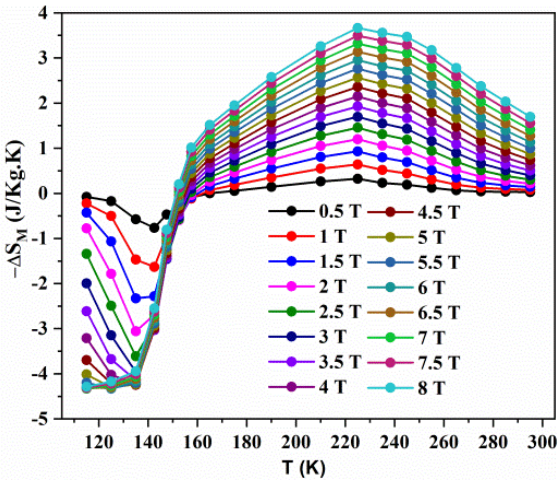

Fig. 9. Temperature dependence of ΔS_M versus T at different (H) calculated from numerical integration of Maxwell relation.

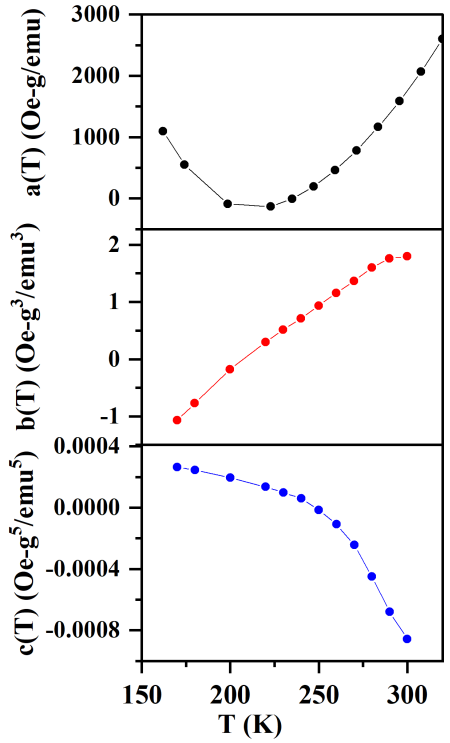

Fig. 10. Temperature dependence of Landau coefficient $a(T)$, $b(T)$, and $c(T)$.

using the $M(\mu_0 H, T)$ data [26], [25]

$$S_M(T, H) = S_M(T, H_1) - S_M(T, H_2) = \int_{H1}^{H2} \left(\frac{\partial M}{\partial T}\right) dH. \quad (2)$$

The integral in (2) could be roughly represented as when the magnetic field and temperature are present in small discrete intervals, given by the following equation:

$$\Delta S_M(T, H) = \sum_i \frac{M_i - M_{i+1}}{T_i - T_{i+1}} \Delta H_i. \quad (3)$$

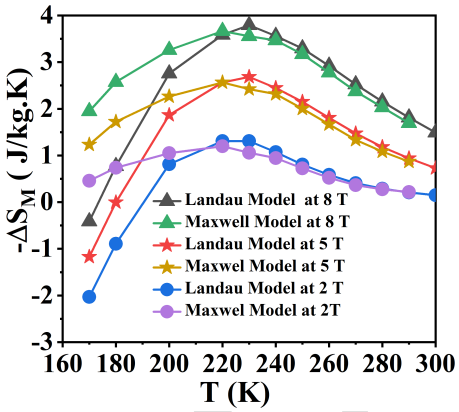

Fig. 11. Comparison of ΔS_M calculated from Maxwell and Landau model.

TABLE I
COMPARISON RESULTS OF MAGNETIC ENTROPY CHANGE AT T_c AND T_N

Sample	(-)ΔSm (Tc)(J/Kg K) (H=5 T)	ΔSm(T_N) (J/Kg K) (H=5 T)	Tc (K)	T_N (K)	Ref.
$Pr_{0.5}Sr_{0.5}MnO_3$	3.20	7.50	255	165	[9]
$Pr_{0.5}Sr_{0.5}MnO_3$	1.90	---	268	90	[29]
$Pr_{0.5}Sr_{0.5}MnO_3$ (SG)	2.20	2.20	265	85	[8]
$Pr_{0.5}Sr_{0.5}MnO_3$ (SSR)	3.26	7.86	243	159	[8]
$Pr_{0.5}Sr_{0.5}MnO_3$ (~44 nm)	2.27	4.46	250	178	[30]
$Pr_{0.5}Sr_{0.5}MnO_3$ (~39 nm)	2.57	6.27	240	180	[30]
$Pr_{0.5}Sr_{0.5}MnO_3$ (~36 nm)	2.58	6.42	235	185	[30]
$Pr_{0.46}Sr_{0.54}MnO_3$	--	8.00	--	210	[12]
$Pr_{0.48}Sr_{0.52}MnO_3$	2.56 (5T) 3.67 (8T)	4.29	226	152.5	This Work

The model suggested that the absolute value of $|\Delta S_M|$ rises as the field is increased, which is obvious due enhancement of FM interaction with the increase in the magnetic field as shown in Fig. 9.

Furthermore, two maxima: one near T_c and has a negative value and the other in the proximity of the FM–AFM transition temperature and has a positive value. The negative maximum $\Delta S_M = 3.67$ J Kg^{-1}K^{-1} has been observed for a magnetic field of 8 T at $T_c = 226$ K and the positive maximum value of ΔS_M can be witnessed in the proximity of T_N with a value of $+4.29$ J Kg^{-1} K^{-1} at merely the magnetic field of 5 T, which significantly remained unchanged with the increasing field up to 8 T. The substantial ΔS_M value recorded at T_N is attributable to the FOPT characteristic of the meta-magnetic transition in the sample. Table I presents the comparison results of ΔS_M at T_c and T_N for PSMO samples near half doping. It can be seen that the ΔS_M, T_c, and T_N are not consistent and depends upon the synthesis condition as well as the grain size.

Taking the Landau model to realize the significance of MCE, the theory is used to determine the nature of a SOPT and FOPT [25], taking the contribution of magneto elastic and electron interaction. By neglecting higher-order parts in the Landau power expansion of the magnetization M, the

Gibbs free energy versus magnetization and temperature can be expressed in the following equation [27], [28]:

$$G(M,T) = G(0) + \frac{a(T)}{2}M^2 + \frac{b(T)}{4}M^4 + \frac{c(T)}{6}M^6 + \cdots - M\mu_o H \quad (4)$$

where $a(T)$, $b(T)$, and $c(T)$ are the temperature-dependent Landau coefficients representing the magneto-elastic coupling and the electron scattering energy. From the equilibrium energy minimization $(\partial G/\partial M) = 0$, (4) can be written as follows:

$$\frac{\mu_0 H}{M} = a(T) + b(T)M^2 + c(T)M^4. \quad (5)$$

Further, (5) is as follows:

$$\mu_0 H = a(T)M + b(T)M^3 + c(T)M^5. \quad (6)$$

From (6), the values of $a(T)$, $b(T)$, and $c(T)$ can be calculated by fitting magnetization isothermal data. The magnetic entropy is calculated by differentiating the Gibbs free energy from the temperature

$$S_M(T,H) = -\left(\frac{G(H,T)}{T}\right) = \frac{a'(T)}{2}M^2 - \frac{b'(T)}{4}M^4 - \frac{c'(T)}{6}M^6 \quad (7)$$

where $a'(T)$, $b'(T)$, and $c'(T)$ are the temperature derivative of the Landau coefficient. Fig. 10 shows the dependence of "a" on temperature (T) is positive and minimum in the proximity of T_c in agreement with FM characteristics. The positive sign of the Landau coefficient $b(T_c)$ confirmed that the magnetic phase transition is SOPT and the $c(T)$ parameter is generally positive in low-temperature regions and becomes negative with increasing temperature.

The calculated ΔS_M values calculated using Maxwell's model and Landau's theory, at different temperatures (T) near SOPT (T_c) and the magnetic fields of 2, 5, and 8 T are shown in Fig. 11. The magnetic entropy change (ΔS_M) estimated from Landau and Maxwell's model is in the good agreement above T_c (PM region), however, shows deviation below T_c (FM region). This observation suggests that the magnetic entropy significantly depends on temperature and that the contribution of the electron interaction and the magneto-elastic coupling is auxiliary.

Furthermore, the observed deviation in magnetic entropy change at low temperatures can also attribute to the fact that the Landau theory is unable to account for the probable effect of exchange interactions and Jahn–Teller distortion, which are prevalent in the case of manganite [27].

III. Conclusion

The dual magnetic phase transition; FOPT AFM/CO-FM transition at $T_{CO} = T_N = 150$ K pursued by a SOPT FM–PM transition at $T_C = 226$ K. A comparison of theoretically (Landau model) calculated and experimentally (Maxwell's relation) obtained ΔS_M established that the electron interaction and magneto-elastic coupling are dominant origins to surmise the significance of ΔS_M.

Acknowledgment

This work was supported by the Collaborative Research Scheme (CSR-IC/CRS-89) of UGC-DAE-CSR, Indore Centre to VD. Ajay Kumar Saw would like to thank UGC DAE CSR and MRF for fellowship. They are gratified to scientists of UGC-DAE-CSR, Indore Centre; Dr. Rajeev Rawat (PC) for the scheme for electrical and magneto-transport measurements, and Dr. Alok Banerjee and Kranti Kumar for magnetic measurements; Dr. Mukul Gupta and Layanta Behera for X-ray diffraction (XRD). There gratefully acknowledge Dr. R. J. Choudhary and Dr. D. M. Phase for the X-ray absorption spectra (XAS) facility at Indus 2 RRCAT, Indore.

References

[1] M. M. Savosta, V. A. Borodin, M. Marysko, Z. Jirák, J. Hejtmánek, and P. Novák, "Ferromagnetic–antiferromagnetic transition in $Pr_{0.51}Sr_{0.49}MnO_3$ manganite," *Phys. Rev. B, Condens. Matter*, vol. 65, no. 22, p. 6366, Jun. 2002, doi: 10.1103/PhysRevB.65.224418.

[2] M. Fries, K. P. Skokov, D. Y. Karpenkov, V. Franco, S. Ener, and O. Gutfleisch, "The influence of magnetocrystalline anisotropy on the magnetocaloric effect: A case study on Co_2B," *Appl. Phys. Lett.*, vol. 109, no. 23, Dec. 2016, Art. no. 232406, doi: 10.1063/1.4971839.

[3] M. Hsini, S. Hcini, and S. Zemni, "Magnetocaloric effect simulation by Landau theory and mean-field approximation in $Pr_{0.5}Sr_{0.5}MnO_3$," *Eur. Phys. J. Plus*, vol. 134, no. 12, p. 588, Dec. 2019, doi: 10.1140/epjp/i2019-12975-4.

[4] E. Palacios, C. Tomasi, R. Sáez-Puche, A. J. Dos Santos-García, F. Fernández-Martínez, and R. Burriel, "Effect of Gd polarization on the large magnetocaloric effect of $GdCrO_4$ in a broad temperature range," *Phys. Rev. B, Condens. Matter*, vol. 93, no. 6, pp. 1–8, Feb. 2016, doi: 10.1103/PhysRevB.93.064420.

[5] P. Sande et al., "Large magnetocaloric effect in manganites with charge order," *Appl. Phys. Lett.*, vol. 79, no. 13, pp. 2040–2042, 2001, doi: 10.1063/1.1403317.

[6] M. S. Reis, A. M. Gomes, J. P. Araujo, P. B. Tavares, I. S. Oliveira, and V. S. Amaral, "Positive and 'colossal' magnetocaloric effect due to charge ordering in CMR manganites," *J. Magn. Magn. Mater.*, vols. 272–276, pp. 2393–2394, May 2004, doi: 10.1016/j.jmmm.2003.12.650.

[7] S. Karmakar, E. Bose, S. Taran, B. K. Chaudhuri, C. P. Sun, and H. D. Yang, "Magnetocaloric effect in charge ordered $Nd_{0.5}Ca_{0.5}MnO_3$ manganite," *J. Appl. Phys.*, vol. 103, no. 2, 2008, Art. no. 023901 , doi: 10.1063/1.2827117.

[8] A. Sakka et al., "Impact of synthesis routes on normal and inverse magnetocaloric effects and critical behaviour in the charge-ordered $Pr_{0.5}Sr_{0.5}MnO_3$ manganite," *Eur. Phys. J. Plus*, vol. 134, no. 5, pp. 1–17, May 2019, doi: 10.1140/epjp/i2019-12615-1.

[9] N. S. Bingham, M. H. Phan, H. Srikanth, M. A. Torija, and C. Leighton, "Magnetocaloric effect and refrigerant capacity in charge-ordered manganites," *J. Appl. Phys.*, vol. 106, no. 2, Jul. 2009, Art. no. 023909, doi: 10.1063/1.3174396.

[10] A. Biswas, T. Samanta, S. Banerjee, and I. Das, "Observation of large low field magnetoresistance and large magnetocaloric effects in polycrystalline $Pr_{0.65}(Ca_{0.7}Sr_{0.3})_{0.35}MnO_3$," *Appl. Phys. Lett.*, vol. 92, no. 1, 2008, Art. no. 012502, doi: 10.1063/1.2828980.

[11] P. Amirzadeh et al., "Phase separation and direct magnetocaloric effect in $La_{0.5}Ca_{0.5}MnO_3$ manganite," *J. Appl. Phys.*, vol. 113, no. 12, 2013, Art. no. 123904, doi: 10.1063/1.4794179.

[12] V. B. Naik, S. K. Barik, R. Mahendiran, and B. Raveau, "Magnetic and calorimetric investigations of inverse magnetocaloric effect in $Pr_{0.46}Sr_{0.54}MnO_3$," *Appl. Phys. Lett.*, vol. 98, no. 11, 2011, Art. no. 112506, doi: 10.1063/1.3567760.

[13] L. B. Mccusker et al., "Rietveld refinement guidelines," *J. Appl. Crystallogr.*, vol. 32, no. 1, pp. 36–50, 1999, doi: 10.1107/S0021889898009856.

[14] G. Subias, J. Garcia, M. C. Sanchez, J. Blasco, and M. G. Proietti, "Soft X-ray absorption spectroscopy ($MnL_{2,3}$ and OK) in mixed valence manganites," *Surf. Rev. Lett.*, vol. 9, no. 2, pp. 1071–1078, Apr. 2002.

[15] Y. Tomioka, A. Asamitsu, Y. Moritomo, H. Kuwahara, and Y. Tokura, "Collapse of a charge-ordered state under a magnetic field in $Pr_{1/2}Sr_{1/2}MnO_3$," *Phys. Rev. Lett.*, vol. 74, no. 25, p. 5108, 1995.

[16] C. Zener, "Interaction between *d*-shells in the transition metals. II. Ferromagnetic compounds of manganese with perovskite structure," *Phys. Rev.*, vol. 82, no. 3, pp. 403–405, May 1951, doi: 10.1103/PhysRev.82.403.

[17] A. A. Hossain et al., "Influence of grain size on magnetoresistance properties of bulk $La_{0.67}Ca_{0.33}MnO_{3-\delta}$," *J. Magn. Magn. Mater.*, vol. 192, no. 2, pp. 263–270, 1999, doi: 10.1016/S0304-8853(98)00530-7.

[18] A. Gupta et al., "Grain-boundary effects on the magnetoresistance properties of perovskite manganite films," *Phys. Rev. B, Condens. Matter*, vol. 54, no. 22, pp. 15629–15632, Dec. 1996, doi: 10.1103/PhysRevB.54.R15629.

[19] D. Emin and N. L. H. Liu, "Small-polaron hopping in magnetic semiconductors," *Phys. Rev. B, Condens. Matter*, vol. 27, no. 8, pp. 4788–4798, Apr. 1983, doi: 10.1103/PhysRevB.27.4788.

[20] S. Keshri, V. Dayal, and L. Joshi, "Influence of Fe doping on electrical properties of LCMO," *Phase Transitions*, vol. 81, no. 1, pp. 17–28, Jan. 2008, doi: 10.1080/01411590701448772.

[21] A. K. Saw, S. Hunagund, R. L. Hadimani, and V. Dayal, "Magnetic phase transition, magnetocaloric and magnetotransport properties in $Pr_{0.55}Sr_{0.45}MnO_3$ perovskite manganite," *Mater. Today Proc.*, vol. 46, pp. 6218–6222, Jan. 2020, doi: 10.1016/j.matpr.2020.04.766.

[22] H. E. Sekrafi, A. Ben Jazia Kharrat, N. Chniba-Boudjada, and W. Boujelben, "Impact of B-site doping on magnetic and magnetocaloric effect of $Pr_{0.75}Bi_{0.05}Sr_{0.1}Ba_{0.1}Mn_{1-x}TixO_3$ ($0\leq x \leq 0.04$) manganites," *Solid State Sci.*, vol. 105, Jul. 2020, Art. no. 106274, doi: 10.1016/j.solidstatesciences.2020.106274.

[23] S. K. Banerjee, "On a generalised approach to first and second order magnetic transitions," *Phys. Lett.*, vol. 12, no. 1, pp. 16–17, 1964, doi: 10.1016/0031-9163(64)91158-8.

[24] A. H. El-Sayed and M. A. Hamad, "Phenomenological modeling of magnetocaloric effect in $La_{0.7}Sr_xMnO_{3-\delta}$," *J. Supercond. Novel Magn.*, vol. 31, no. 10, pp. 3357–3360, Oct. 2018, doi: 10.1007/s10948-018-4605-z.

[25] M. Hsini, S. Hcini, and S. Zemni, "Magnetocaloric effect studying by means of theoretical models in $Pr_{0.5}Sr_{0.5}MnO_3$ manganite," *J. Magn. Magn. Mater.*, vol. 466, pp. 368–375, Nov. 2018, doi: 10.1016/j.jmmm.2018.07.051.

[26] J. S. Amaral and V. S. Amaral, "On estimating the magnetocaloric effect from magnetization measurements," *J. Magn. Magn. Mater.*, vol. 322, nos. 9–12, pp. 1552–1557, May 2010, doi: 10.1016/j.jmmm.2009.06.013.

[27] B. Biswas, R. Nag, M. Debnath, S. Taran, and S. Pal, "Magnetic and magnetocaloric properties of monovalent (Li^{+1}) doped $PrMnO_3$: A study by Maxwell relation and Landau theory," *Appl. Phys. A*, vol. 128, no. 7, pp. 1–8, Jul. 2022, doi: 10.1007/s00339-022-05696-6.

[28] K. Dhahri et al., "Magnetic, magnetocaloric and critical behavior investigation of $La_{0.7}Ca_{0.1}Pb_{0.2}Mn_{1-x-y}Al_xSnyO_3$ (x, y = 0.0, 0.05 and 0.075) prepared by a sol–gel method," *RSC Adv.*, vol. 7, no. 69, pp. 43410–43423, 2017, doi: 10.1039/c7ra03913a.

[29] S. Tarhouni et al., "Structural, magnetic and magnetocaloric properties of Ag-doped $Pr_{0.5}Sr_{0.5-x}Ag_xMnO_3$ manganites ($0.0\leq x \leq 0.4$)," *Ceram. Int.*, vol. 43, no. 1, pp. 133–143, Jan. 2017, doi: 10.1016/j.ceramint.2016.09.122.

[30] M. Bourouina, A. Krichene, N. C. Boudjada, M. Khitouni, and W. Boujelben, "Structural, magnetic and magnetocaloric properties of nanostructured $Pr_{0.5}Sr_{0.5}MnO_3$ manganite synthesized by mechanical alloying," *Ceramics Int.*, vol. 43, no. 11, pp. 8139–8145, 2017, doi: 10.1016/j.ceramint.2017.03.138.

Other Corrections:

Page and line no.	Incorrect Word or Sentence	Correction in Word/Sentence
Page2, Line 76	Costate	CO state
Page 2, Line 119	at 500 Oe magnetic field	at 500 Oe magnetic field
Page 5, line 191	(4) can	eq.(4) can..
Page 5, line 194	Further (5)	Further eq. (5)
Page 5, line 196	From (6)	From eq. 6)
Page 5, line 210	The calculated SM values calculated using Maxwell's model	The calculated SM values using Maxwell's model

AUTHOR QUERIES

AUTHOR PLEASE ANSWER ALL QUERIES

PLEASE NOTE: We cannot accept new source files as corrections for your article. If possible, please annotate the PDF proof we have sent you with your corrections and upload it via the Author Gateway. Alternatively, you may send us your corrections in list format. You may also upload revised graphics via the Author Gateway.

Carefully check the page proofs (and coordinate with all authors); additional changes or updates WILL NOT be accepted after the article is published online/print in its final form. Please check author names and affiliations, funding, as well as the overall article for any errors prior to sending in your author proof corrections.

AQ:1 = Please check the Institute name Maharaja Institute of Technology Mysore, (VTU-Belagavi), for correctness and amend if necessary.

AQ:2 = Please confirm the city name for Maharaja Institute of Technology Mysore and Virginia Commonwealth University.

AQ:3 = Please supply index terms/keywords for your article. To download the IEEE Taxonomy, go to http://www.ieee.org/documents/taxonomy_v101.pdf.

AQ:4 = Please confirm or add details for any funding or financial support for the research of this article.

AQ:5 = Please provide the expansions of the acronyms UGC, DAE, CSR, and VD for your funding agency. Providing the correct acknowledgment will ensure proper credit to the funder.

Magnetocaloric Properties of a Charge Ordered $Pr_{0.48}Sr_{0.52}MnO_3$ Perovskite Near First and Second Order Magnetic Transition

Ajay Kumar Saw[1], John Peter J. Nunez[2], Ravi. L. Hadimani[2], and Vijaylakshmi Dayal[1]

[1]Department of Physics, Maharaja Institute of Technology Mysore, (VTU-Belagavi), Mandya 517477, India
[2]Department of Mechanical and Nuclear Engineering, Virginia Commonwealth University, Richmond, VA 23285 USA

Polycrystalline $Pr_{0.48}Sr_{0.52}MnO_3$ forms a tetragonal structure belonging to the I4/mcm space group. X-ray absorption spectroscopy revealed Mn_3d level splitting with a higher density of state in $e_g \downarrow$. The temperature-dependent electrical resistivity plot indicates metal-to-insulator transition (T_{MI}) at 224 K at 0 T. Additionally, at lower temperatures, a distinct thermal hysteresis during heating and cooling cycles between 0 and 2 T fields specifies a first-order (FOPT) magnetic phase transition. The temperature-dependent magnetization plot shows a second-order (SOPT) paramagnetic (PM) to ferromagnetic (FM) transition phase transition at 226 K ($=T_c$) followed by FM to antiferromagnetic (AFM) transition with distinct thermal hysteresis evidence of FOPT at 152.5 K ($=T_N$). The maximum isothermal entropy change (ΔS_M) estimated using Maxwell's model near SOPT is -3.67 J/kg K at 8 T. Moreover, near FOPT the maximum ΔS_M of value $+4.29$ J/kg K at $H = 4$ T is determined, which thereafter remained constant up to 8 T magnetic field. The ΔS_M value at a lower magnetic field is also computed using the phenomenological model. Landau's theory suitably explains the magnetocaloric (MCE) of $Pr_{0.48}Sr_{0.52}MnO_3$ near SOPT in agreement with the value obtained using Maxwell's relation.

***Index Terms*— XXXXX.**

I. Introduction

MANGANITES near half doping are extremely fascinating since competing ferromagnetic metallic (FM-M) and antiferromagnetic (AFM) charge-ordered insulating (COI) phases have an analogous energy scale, implying that both phases potentially coexisted [1]. Furthermore, magnetocaloric (MCE) behavior has been demonstrated in these manganites. Magnetic refrigeration tools, focusing on MCE, is environmentally sustainable and energy efficient than traditional gas compression or expansion refrigeration tools [2], [3], [4]. The MCE, or adiabatic change in temperature (ΔT_{ad}) or isothermal change in magnetic entropy (ΔS_M), is largely been studied in the ferromagnetic (FM) materials at temperatures near second-order (SOPT) paramagnetic (PM) to FM phase transition (SOPT), the AFM materials with first-order (FOPT) FM to AFM-COI phase transition (FOPT) are also investigated for its giant MCE and large ΔS_M values [5], [6], [7], [8], [9], [10], [11], [12]. In this article, we investigated the magneto-transport, magnetic phase transition, and MCE properties of polycrystalline $Pr_{0.48}Sr_{0.52}MnO_3$ synthesized using the solid-state technique.

II. Results and Discussion

A. Structural and Morphological Study

The X-ray diffraction (XRD) plot together with the Rietveld refined pattern of the synthesized samples is shown in Fig. 1.

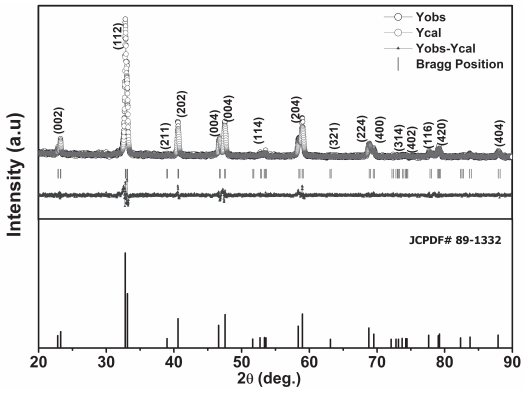

Fig. 1. Experimental XRD pattern along with Rietveld refined pattern.

The pattern suggests the crystallization of the sample in the tetragonal phase (JCPDF# 89–1332) with space group I4/mcm without any secondary phase. The Rietveld refinement was performed using Fullprof software [13]. The lattice parameters acquired using the refinement are, $a = b = 5.407(7)$ (Å), $c = 7.765(2)$ (Å), $V = 227.079(4)$ (Å)^3, Mn-O_1 = 1.941(4) (Å) and Mn_1-O_2-Mn_1 = 126.258 (2)^o.

Fig. 2 displays X-ray absorption spectra (XAS) performed at the Mn L edge. The Mn $L_{2,3}$ edge noted in XAS results from the transition of Mn $2p_{1/2}$ and Mn $2p_{3/2}$ states to the vacant Mn_3d state. The protocol described by Subias et al. [14] has been adopted to investigate the accurate charge state of Mn.

According to this protocol, the L_2 peaks of the samples have been aligned with the energy position of MnO_2 and Mn_2O_3 and the later position of the L_3 peak has been investigated. It can be seen that the L_3 peak position lies between the L_3

Manuscript received 27 March 2023; revised 8 May 2023 and 29 May 2023; accepted 5 June 2023. Corresponding author: V. Dayal (e-mail: drvldayal@gmail.com).

Color versions of one or more figures in this article are available at https://doi.org/10.1109/TMAG.2023.3286435.

Digital Object Identifier 10.1109/TMAG.2023.3286435

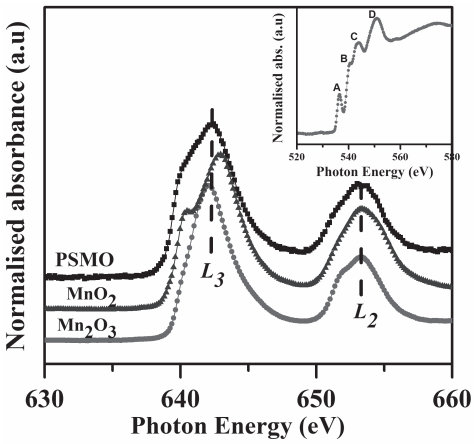

Fig. 2. XAS performed at the MnL edge.

peaks of MnO_2 and Mn_2O_3, suggesting the presence of Mn^{3+} and Mn^{4+} and signifying a mixed valent nature. Additionally, the normalized XAS spectra oxygen $(O)_{1S}$ spectra around the K-edge (in the inset of Fig. 2) show the four distinct bands, where "a" (at 536.52 eV), "c" (at 544.46 eV), and "d" (at 551.25 eV) have been ascribed to the hybridization of O_{2p} with Mn_3d, O_{2p} with Sr_{4d} and O_{2p} with Mn_{4sp}, respectively, whereas "b" (at 540.13 eV), is ascribed to the Mn_3d unoccupied ($e_g \downarrow$) state sensitive to Mn valence, which arises as a result of the splitting of the Mn_3d level. The scanning electron micrograph (SEM) shown in Fig. 3 (left panel) shows densely distributed microns size grains and the energy dispersive X-ray spectrum (EDX) (right panel) suggests the presence of the constituents Pr, Sr, Mn, and O element.

B. Electrical and Magnetotransport Properties

The temperature-dependent resistivity plot as a response to 0 T shown in Fig. 4 shows metal-insulator transition (MI) at $T_{MI} = 224$ K, whereas CO transition at ∼150 K.

Additionally, a distinct thermal hysteresis can be seen during heating and cooling cycles between 0 and 2 T field. This hysteresis is a critical feature of a FOPT with the concomitance of AFM and CO phases, designated to the phase transition to the Costate, where ostensibly Mn^{3+} and Mn^{4+} ions display a real space arrangement in the sample [15]. Furthermore, it has been noticed that the applied magnetic field suppressed the resistivity and shifted the T_{MI} at the higher temperature side, indicating that the magnetic field enables the e_g electrons to hop amid the neighboring Mn ions. This hopping strengthens the double exchange (DE) mechanism, which typically favors the FM nature [16]. FOPT is diminished at the higher field (8 T). The temperature-dependent magnetoresistance (MR)%, which is equal to $(\rho H - \rho 0/\rho 0) \times 100$ (as shown in the right scale of Fig. 4) increases by lowering the temperature and applying the magnetic field. MR of ∼ 100% has been observed at 5 K and 8 T, which seems to be significant for magnetic device applications. Furthermore, the MR% isotherms, under magnetic fields (0–8 T) are shown in Fig. 5. At 5 and 100 K, the thermal hysteresis in cycles 0–8 T and 8–0 T is seen, which indicates that magnetic fields have caused the CO-I phase to

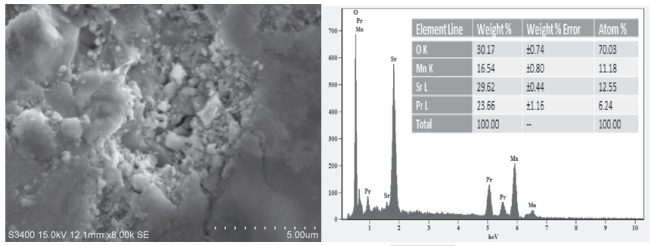

Fig. 3. SEM (left panel) and EDX spectrum (right panel) of the sample.

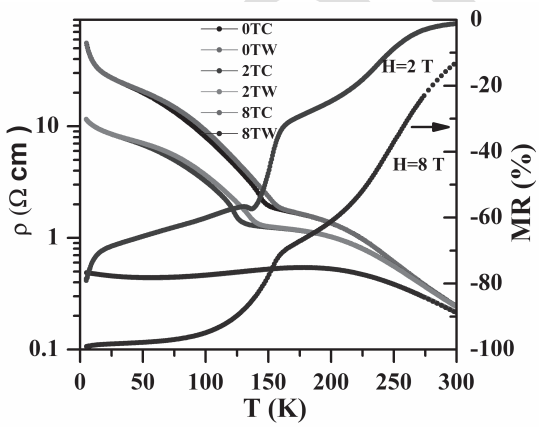

Fig. 4. Resistivity versus temperature plot in left axis and right axis shows MR% versus T.

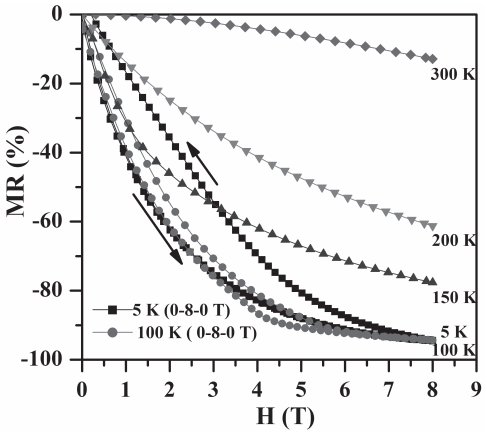

Fig. 5. MR% versus the magnetic field (H) isotherms measured at 5, 100, 150, 200, and 300 K.

destabilize. The dominant low field negative MR along with MR ∼ 96% is measured at the temperature at both 5 and 100 K at 8 T. At temperatures well below T_{MI}, it is understood that the FMM phase fraction is significantly greater compared to the COI phase, which results in the low field MR primarily by the grain boundary effect [17], [18].

The adiabatic small polaronic hopping (SPH) model given by (1) is seen to be dominant at a high temperature as shown in Fig. 6 [19], [20], [2]

$$\rho = \rho_0 T_{\exp}\left(\frac{E_a}{K_B T}\right). \quad (1)$$

Here, E_a = activation energy, K_B = Boltzmann's constant, and ρ_0 = residual resistivity coefficient term designated by

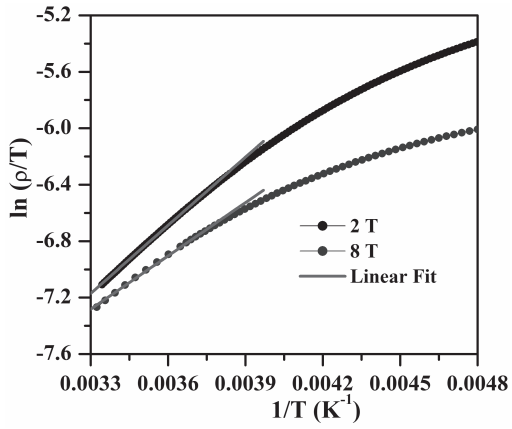

Fig. 6. Plot of $\ln(\rho/T)$ versus 1/T (solid lines indicate linear fits with the SPH model).

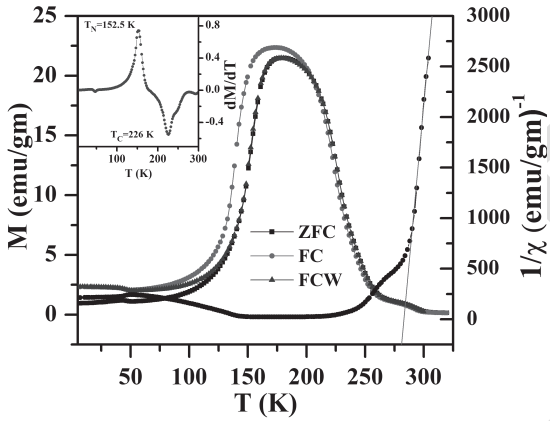

Fig. 7. Temperature dependence of ZFC, FC, and FCW magnetization measured at 500 Oe (Left axis). (Right axis) $1/\chi$ versus T in an applied magnetic field. The inset shows the derivative of magnetization.

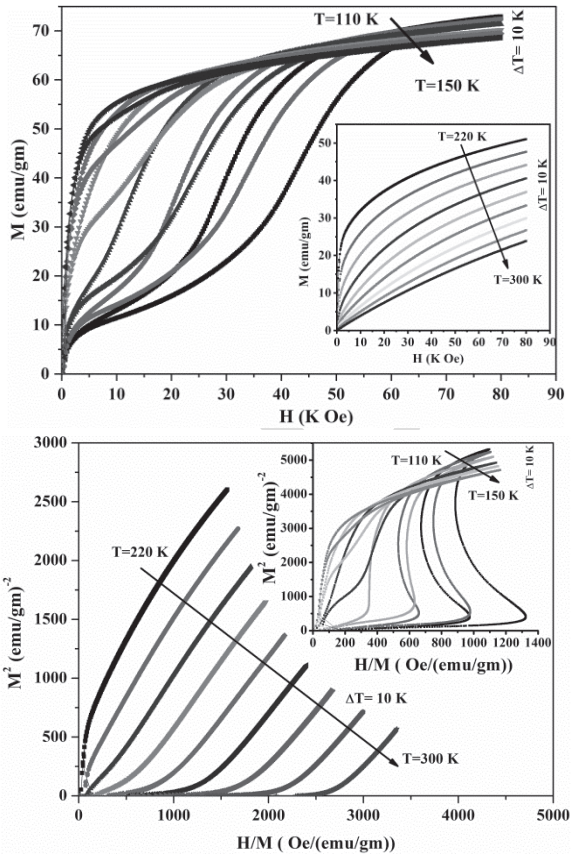

Fig. 8. (Top panel) Magnetic field dependence of magnetization at different temperatures (bottom panel). Arrott's plot at different temperatures.

$\rho_0 = 2K_BT/3ne^2a^2v$, where e = electronic charge, n = density of charge carrier, a = site-to-site hopping distance, and v = longitudinal phonon frequency. The application of the magnetic field decreased the activation energy (E_a) from 138.74 (0 T) to 108.493 meV (8 T).

It is presumed that the application of magnetic decreases E_a value due to a decrease in the distortion of the lattice and the decline in Jahn–Teller electron–phonon coupling, causing the electrons to become delocalized, which is following $\rho(T)$ data, which decreases when the magnetic field is applied.

C. Magnetic and MCE Properties

The zero-field-cooled (ZFC), field-cooled (FC), and FC warming (FCW) magnetization (M) as a response to temperature (T) at 500 Oe magnetic is shown in Fig. 7. The plot shows that the sample undergoes a dual transition; a PM to FM state SOPT at $T_C = 226$ K followed by FM to AFM state (FOPT) at $T_N = 152.5$ K. The Curie–Weiss law fitting to the PM region, the θ_{cw} (=282.6 K) acquired a positive value and corroborates the FM nature of the sample above T_N, however, a slightly higher θ_{cw} value than T_c (226 K) is a signature of a magnetic inhomogeneity in the sample, also higher $\mu_{\text{eff}}^{\text{exp}}$ (3.73 μ_B) than the expected $\mu_{\text{eff}}^{\text{Th}}$ (3.51 μ_B) value confirmed the manifestation of magnetic inhomogeneity just beyond T_c [21], [22].

Furthermore, the magnetic field dependence of magnetization (M versus H isotherms) measured in the temperature range 110–180 K and from 220 to 300 K for a temperature interval of $\Delta T = 10$ K are shown in Fig. 8 (top panel).

It can be noticed that the $M(H)$ data below T_c surges faster at the lower field region and then appears to saturate as the magnetic field is increased. Arrott's plot (M^2 versus H/M) is studied to comprehend magnetic transitions, as shown in Fig. 8 (bottom panel). As per Banerjee [23] criterion, the negative and positive signs of the slope in the Arrotts plot are signatures of the magnetic phase transition resembling FOPT and SOPT, respectively. The magnetic isotherms plot discloses FOPT below 152.5 K and SOPT above 152.5 K in agreement with the temperature-dependent ZFC-FC magnetization measurements.

To further study the MCE behavior, magnetic entropy change (ΔS_M) as a function of temperature and magnetic field has been largely discussed considering various models, such as; phenomenological [24], Maxwell's, and Landau's theory [25]. Using the phenomenological model of the MCE in the magnetic materials at the low field ($H = 0.05$ T), the temperature-dependent magnetization showed ΔS_M to be maximum near $T_N = 152.5$ K, $T_C = 226$ K. Further, in Maxwell's model, based on the thermodynamic theory, the magnetic entropy change (ΔS_M) can be calculated

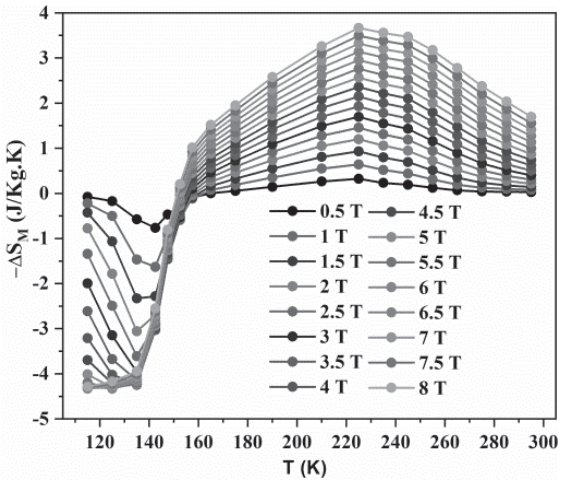

Fig. 9. Temperature dependence of ΔS_M versus T at different (H) calculated from numerical integration of Maxwell relation.

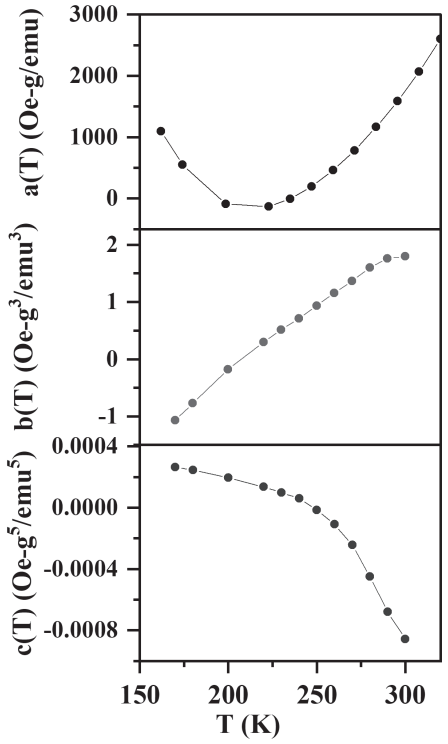

Fig. 10. Temperature dependence of Landau coefficient $a(T)$, $b(T)$, and $c(T)$.

using the $M(\mu_0 H, T)$ data [26], [25]

$$S_M(T, H) = S_M(T, H_1) - S_M(T, H_2) = \int_{H1}^{H2} \left(\frac{\partial M}{\partial T}\right) dH. \tag{2}$$

The integral in (2) could be roughly represented as when the magnetic field and temperature are present in small discrete intervals, given by the following equation:

$$\Delta S_M(T, H) = \sum_i \frac{M_i - M_{i+1}}{T_i - T_{i+1}} \Delta H_i. \tag{3}$$

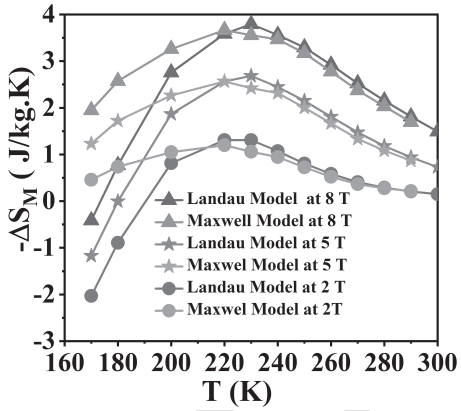

Fig. 11. Comparison of ΔS_M calculated from Maxwell and Landau model.

TABLE I
COMPARISON RESULTS OF MAGNETIC ENTROPY CHANGE AT T_c AND T_N

Sample	(-)ΔSm (Tc)(J/Kg K) (H=5 T)	ΔSm(T_N) (J/Kg K) (H=5 T)	Tc (K)	T_N (K)	Ref.
$Pr_{0.5}Sr_{0.5}MnO_3$	3.20	7.50	255	165	[9]
$Pr_{0.5}Sr_{0.5}MnO_3$	1.90	---	268	90	[29]
$Pr_{0.5}Sr_{0.5}MnO_3$ (SG)	2.20	2.20	265	85	[8]
$Pr_{0.5}Sr_{0.5}MnO_3$ (SSR)	3.26	7.86	243	159	[8]
$Pr_{0.5}Sr_{0.5}MnO_3$ (~44 nm)	2.27	4.46	250	178	[30]
$Pr_{0.5}Sr_{0.5}MnO_3$ (~39 nm)	2.57	6.27	240	180	[30]
$Pr_{0.5}Sr_{0.5}MnO_3$ (~36 nm)	2.58	6.42	235	185	[30]
$Pr_{0.46}Sr_{0.54}MnO_3$	--	8.00	--	210	[12]
$Pr_{0.48}Sr_{0.52}MnO_3$	2.56 (5T) 3.67 (8T)	4.29	226	152.5	This Work

The model suggested that the absolute value of $|\Delta S_M|$ rises as the field is increased, which is obvious due enhancement of FM interaction with the increase in the magnetic field as shown in Fig. 9.

Furthermore, two maxima: one near T_c and has a negative value and the other in the proximity of the FM–AFM transition temperature and has a positive value. The negative maximum $\Delta S_M = 3.67$ J Kg^{-1}K^{-1} has been observed for a magnetic field of 8 T at $T_c = 226$ K and the positive maximum value of ΔS_M can be witnessed in the proximity of T_N with a value of $+4.29$ J Kg^{-1} K^{-1} at merely the magnetic field of 5 T, which significantly remained unchanged with the increasing field up to 8 T. The substantial ΔS_M value recorded at T_N is attributable to the FOPT characteristic of the meta-magnetic transition in the sample. Table I presents the comparison results of ΔS_M at T_c and T_N for PSMO samples near half doping. It can be seen that the ΔS_M, T_c, and T_N are not consistent and depends upon the synthesis condition as well as the grain size.

Taking the Landau model to realize the significance of MCE, the theory is used to determine the nature of a SOPT and FOPT [25], taking the contribution of magneto elastic and electron interaction. By neglecting higher-order parts in the Landau power expansion of the magnetization M, the

Gibbs free energy versus magnetization and temperature can be expressed in the following equation [27], [28]:

$$G(M,T) = G(0) + \frac{a(T)}{2}M^2 + \frac{b(T)}{4}M^4 + \frac{c(T)}{6}M^6 + \cdots - M\mu_o H \quad (4)$$

where $a(T)$, $b(T)$, and $c(T)$ are the temperature-dependent Landau coefficients representing the magneto-elastic coupling and the electron scattering energy. From the equilibrium energy minimization $(\partial G/\partial M) = 0$, (4) can be written as follows:

$$\frac{\mu_0 H}{M} = a(T) + b(T)M^2 + c(T)M^4. \quad (5)$$

Further, (5) is as follows:

$$\mu_0 H = a(T)M + b(T)M^3 + c(T)M^5. \quad (6)$$

From (6), the values of $a(T)$, $b(T)$, and $c(T)$ can be calculated by fitting magnetization isothermal data. The magnetic entropy is calculated by differentiating the Gibbs free energy from the temperature

$$S_M(T,H) = -\left(\frac{G(H,T)}{T}\right) = \frac{a'(T)}{2}M^2 - \frac{b'(T)}{4}M^4 - \frac{c'(T)}{6}M^6 \quad (7)$$

where $a'(T)$, $b'(T)$, and $c'(T)$ are the temperature derivative of the Landau coefficient. Fig. 10 shows the dependence of "a" on temperature (T) is positive and minimum in the proximity of T_c in agreement with FM characteristics. The positive sign of the Landau coefficient $b(T_c)$ confirmed that the magnetic phase transition is SOPT and the $c(T)$ parameter is generally positive in low-temperature regions and becomes negative with increasing temperature.

The calculated ΔS_M values calculated using Maxwell's model and Landau's theory, at different temperatures (T) near SOPT (T_c) and the magnetic fields of 2, 5, and 8 T are shown in Fig. 11. The magnetic entropy change (ΔS_M) estimated from Landau and Maxwell's model is in the good agreement above T_c (PM region), however, shows deviation below T_c (FM region). This observation suggests that the magnetic entropy significantly depends on temperature and that the contribution of the electron interaction and the magneto-elastic coupling is auxiliary.

Furthermore, the observed deviation in magnetic entropy change at low temperatures can also attribute to the fact that the Landau theory is unable to account for the probable effect of exchange interactions and Jahn–Teller distortion, which are prevalent in the case of manganite [27].

III. Conclusion

The dual magnetic phase transition; FOPT AFM/CO-FM transition at $T_{CO} = T_N = 150$ K pursued by a SOPT FM–PM transition at $T_C = 226$ K. A comparison of theoretically (Landau model) calculated and experimentally (Maxwell's relation) obtained ΔS_M established that the electron interaction and magneto-elastic coupling are dominant origins to surmise the significance of ΔS_M.

Acknowledgment

This work was supported by the Collaborative Research Scheme (CSR-IC/CRS-89) of UGC-DAE-CSR, Indore Centre to VD. Ajay Kumar Saw would like to thank UGC DAE CSR and MRF for fellowship. They are gratified to scientists of UGC-DAE-CSR, Indore Centre; Dr. Rajeev Rawat (PC) for the scheme for electrical and magneto-transport measurements, and Dr. Alok Banerjee and Kranti Kumar for magnetic measurements; Dr. Mukul Gupta and Layanta Behera for X-ray diffraction (XRD). There gratefully acknowledge Dr. R. J. Choudhary and Dr. D. M. Phase for the X-ray absorption spectra (XAS) facility at Indus 2 RRCAT, Indore.

References

[1] M. M. Savosta, V. A. Borodin, M. Marysko, Z. Jirák, J. Hejtmánek, and P. Novák, "Ferromagnetic–antiferromagnetic transition in $Pr_{0.51}Sr_{0.49}MnO_3$ manganite," *Phys. Rev. B, Condens. Matter*, vol. 65, no. 22, p. 6366, Jun. 2002, doi: 10.1103/PhysRevB.65.224418.

[2] M. Fries, K. P. Skokov, D. Y. Karpenkov, V. Franco, S. Ener, and O. Gutfleisch, "The influence of magnetocrystalline anisotropy on the magnetocaloric effect: A case study on Co_2B," *Appl. Phys. Lett.*, vol. 109, no. 23, Dec. 2016, Art. no. 232406, doi: 10.1063/1.4971839.

[3] M. Hsini, S. Hcini, and S. Zemni, "Magnetocaloric effect simulation by Landau theory and mean-field approximation in $Pr_{0.5}Sr_{0.5}MnO_3$," *Eur. Phys. J. Plus*, vol. 134, no. 12, p. 588, Dec. 2019, doi: 10.1140/epjp/i2019-12975-4.

[4] E. Palacios, C. Tomasi, R. Sáez-Puche, A. J. Dos Santos-García, F. Fernández-Martínez, and R. Burriel, "Effect of Gd polarization on the large magnetocaloric effect of $GdCrO_4$ in a broad temperature range," *Phys. Rev. B, Condens. Matter*, vol. 93, no. 6, pp. 1–8, Feb. 2016, doi: 10.1103/PhysRevB.93.064420.

[5] P. Sande et al., "Large magnetocaloric effect in manganites with charge order," *Appl. Phys. Lett.*, vol. 79, no. 13, pp. 2040–2042, 2001, doi: 10.1063/1.1403317.

[6] M. S. Reis, A. M. Gomes, J. P. Araujo, P. B. Tavares, I. S. Oliveira, and V. S. Amaral, "Positive and 'colossal' magnetocaloric effect due to charge ordering in CMR manganites," *J. Magn. Magn. Mater.*, vols. 272–276, pp. 2393–2394, May 2004, doi: 10.1016/j.jmmm.2003.12.650.

[7] S. Karmakar, E. Bose, S. Taran, B. K. Chaudhuri, C. P. Sun, and H. D. Yang, "Magnetocaloric effect in charge ordered $Nd_{0.5}Ca_{0.5}MnO_3$ manganite," *J. Appl. Phys.*, vol. 103, no. 2, 2008, Art. no. 023901 , doi: 10.1063/1.2827117.

[8] A. Sakka et al., "Impact of synthesis routes on normal and inverse magnetocaloric effects and critical behaviour in the charge-ordered $Pr_{0.5}Sr_{0.5}MnO_3$ manganite," *Eur. Phys. J. Plus*, vol. 134, no. 5, pp. 1–17, May 2019, doi: 10.1140/epjp/i2019-12615-1.

[9] N. S. Bingham, M. H. Phan, H. Srikanth, M. A. Torija, and C. Leighton, "Magnetocaloric effect and refrigerant capacity in charge-ordered manganites," *J. Appl. Phys.*, vol. 106, no. 2, Jul. 2009, Art. no. 023909, doi: 10.1063/1.3174396.

[10] A. Biswas, T. Samanta, S. Banerjee, and I. Das, "Observation of large low field magnetoresistance and large magnetocaloric effects in polycrystalline $Pr_{0.65}(Ca_{0.7}Sr_{0.3})_{0.35}MnO_3$," *Appl. Phys. Lett.*, vol. 92, no. 1, 2008, Art. no. 012502, doi: 10.1063/1.2828980.

[11] P. Amirzadeh et al., "Phase separation and direct magnetocaloric effect in $La_{0.5}Ca_{0.5}MnO_3$ manganite," *J. Appl. Phys.*, vol. 113, no. 12, 2013, Art. no. 123904, doi: 10.1063/1.4794179.

[12] V. B. Naik, S. K. Barik, R. Mahendiran, and B. Raveau, "Magnetic and calorimetric investigations of inverse magnetocaloric effect in $Pr_{0.46}Sr_{0.54}MnO_3$," *Appl. Phys. Lett.*, vol. 98, no. 11, 2011, Art. no. 112506, doi: 10.1063/1.3567760.

[13] L. B. Mccusker et al., "Rietveld refinement guidelines," *J. Appl. Crystallogr.*, vol. 32, no. 1, pp. 36–50, 1999, doi: 10.1107/S0021889898009856.

[14] G. Subias, J. Garcia, M. C. Sanchez, J. Blasco, and M. G. Proietti, "Soft X-ray absorption spectroscopy ($MnL_{2,3}$ and OK) in mixed valence manganites," *Surf. Rev. Lett.*, vol. 9, no. 2, pp. 1071–1078, Apr. 2002.

[15] Y. Tomioka, A. Asamitsu, Y. Moritomo, H. Kuwahara, and Y. Tokura, "Collapse of a charge-ordered state under a magnetic field in $Pr_{1/2}Sr_{1/2}MnO_3$," *Phys. Rev. Lett.*, vol. 74, no. 25, p. 5108, 1995.

[16] C. Zener, "Interaction between *d*-shells in the transition metals. II. Ferromagnetic compounds of manganese with perovskite structure," *Phys. Rev.*, vol. 82, no. 3, pp. 403–405, May 1951, doi: 10.1103/PhysRev.82.403.

[17] A. A. Hossain et al., "Influence of grain size on magnetoresistance properties of bulk $La_{0.67}Ca_{0.33}MnO_{3-\delta}$," *J. Magn. Magn. Mater.*, vol. 192, no. 2, pp. 263–270, 1999, doi: 10.1016/S0304-8853(98)00530-7.

[18] A. Gupta et al., "Grain-boundary effects on the magnetoresistance properties of perovskite manganite films," *Phys. Rev. B, Condens. Matter*, vol. 54, no. 22, pp. 15629–15632, Dec. 1996, doi: 10.1103/PhysRevB.54.R15629.

[19] D. Emin and N. L. H. Liu, "Small-polaron hopping in magnetic semiconductors," *Phys. Rev. B, Condens. Matter*, vol. 27, no. 8, pp. 4788–4798, Apr. 1983, doi: 10.1103/PhysRevB.27.4788.

[20] S. Keshri, V. Dayal, and L. Joshi, "Influence of Fe doping on electrical properties of LCMO," *Phase Transitions*, vol. 81, no. 1, pp. 17–28, Jan. 2008, doi: 10.1080/01411590701448772.

[21] A. K. Saw, S. Hunagund, R. L. Hadimani, and V. Dayal, "Magnetic phase transition, magnetocaloric and magnetotransport properties in $Pr_{0.55}Sr_{0.45}MnO_3$ perovskite manganite," *Mater. Today Proc.*, vol. 46, pp. 6218–6222, Jan. 2020, doi: 10.1016/j.matpr.2020.04.766.

[22] H. E. Sekrafi, A. Ben Jazia Kharrat, N. Chniba-Boudjada, and W. Boujelben, "Impact of B-site doping on magnetic and magnetocaloric effect of $Pr_{0.75}Bi_{0.05}Sr_{0.1}Ba_{0.1}Mn_{1-x}TixO_3$ ($0\leq x \leq 0.04$) manganites," *Solid State Sci.*, vol. 105, Jul. 2020, Art. no. 106274, doi: 10.1016/j.solidstatesciences.2020.106274.

[23] S. K. Banerjee, "On a generalised approach to first and second order magnetic transitions," *Phys. Lett.*, vol. 12, no. 1, pp. 16–17, 1964, doi: 10.1016/0031-9163(64)91158-8.

[24] A. H. El-Sayed and M. A. Hamad, "Phenomenological modeling of magnetocaloric effect in $La_{0.7}Sr_xMnO_{3-\delta}$," *J. Supercond. Novel Magn.*, vol. 31, no. 10, pp. 3357–3360, Oct. 2018, doi: 10.1007/s10948-018-4605-z.

[25] M. Hsini, S. Hcini, and S. Zemni, "Magnetocaloric effect studying by means of theoretical models in $Pr_{0.5}Sr_{0.5}MnO_3$ manganite," *J. Magn. Magn. Mater.*, vol. 466, pp. 368–375, Nov. 2018, doi: 10.1016/j.jmmm.2018.07.051.

[26] J. S. Amaral and V. S. Amaral, "On estimating the magnetocaloric effect from magnetization measurements," *J. Magn. Magn. Mater.*, vol. 322, nos. 9–12, pp. 1552–1557, May 2010, doi: 10.1016/j.jmmm.2009.06.013.

[27] B. Biswas, R. Nag, M. Debnath, S. Taran, and S. Pal, "Magnetic and magnetocaloric properties of monovalent (Li^{+1}) doped $PrMnO_3$: A study by Maxwell relation and Landau theory," *Appl. Phys. A*, vol. 128, no. 7, pp. 1–8, Jul. 2022, doi: 10.1007/s00339-022-05696-6.

[28] K. Dhahri et al., "Magnetic, magnetocaloric and critical behavior investigation of $La_{0.7}Ca_{0.1}Pb_{0.2}Mn_{1-x-y}Al_xSnyO_3$ (x, y = 0.0, 0.05 and 0.075) prepared by a sol–gel method," *RSC Adv.*, vol. 7, no. 69, pp. 43410–43423, 2017, doi: 10.1039/c7ra03913a.

[29] S. Tarhouni et al., "Structural, magnetic and magnetocaloric properties of Ag-doped $Pr_{0.5}Sr_{0.5-x}Ag_xMnO_3$ manganites ($0.0\leq x \leq 0.4$)," *Ceram. Int.*, vol. 43, no. 1, pp. 133–143, Jan. 2017, doi: 10.1016/j.ceramint.2016.09.122.

[30] M. Bourouina, A. Krichene, N. C. Boudjada, M. Khitouni, and W. Boujelben, "Structural, magnetic and magnetocaloric properties of nanostructured $Pr_{0.5}Sr_{0.5}MnO_3$ manganite synthesized by mechanical alloying," *Ceramics Int.*, vol. 43, no. 11, pp. 8139–8145, 2017, doi: 10.1016/j.ceramint.2017.03.138.

Other Corrections:

Page and line no.	Incorrect Word or Sentence	Correction in Word/Sentence
Page2, Line 76	Costate	CO state
Page 2, Line 119	at 500 Oe magnetic field	at 500 Oe magnetic field
Page 5, line 191	(4) can	eq.(4) can..
Page 5, line 194	Further (5)	Further eq. (5)
Page 5, line 196	From (6)	From eq. 6)
Page 5, line 210	The calculated SM values calculated using Maxwell's model	The calculated SM values using Maxwell's model